Extreme Mass Ratio Inspirals triggered by Massive Black Hole Binaries: from Relativistic Dynamics to Cosmological Rates

Matteo Bonetti - Università degli studi di Milano-Bicocca

Unsolved problems in astrophysics

Unsolved problem: Different formation of Extreme Mass Ratio Inspirals

Matteo Bonetti - Università degli studi di Milano-Bicocca

~~Unsolved problem: Different formation of Extreme Mass Ratio Inspirals~~

Extreme Mass Ratio Inspirals triggered by Massive Black Hole Binaries: from Relativistic Dynamics to Cosmological Rates

UNIVERSITÀ DEGLI STUDI DI MILANO BICOCCA

EPTA

LISA CONSORTIUM

Matteo Bonetti - Università degli studi di Milano-Bicocca

Giovanni Mazzolari

Extreme Mass Ratio Inspirals triggered by Massive Black Hole Binaries: from Relativistic Dynamics to Cosmological Rates.

Giovanni Mazzolari,[1,2,3]★ Matteo Bonetti,[4,5,6]† Alberto Sesana[4,5,6], Riccardo M. Colombo[4], Massimo Dotti[4,5,6], Giuseppe Lodato[3], David Izquierdo-Villalba.[4,5]

[1]*Department of Physics and Astronomy, Alma Mater Studiorum Universitá di Bologna, via Gobetti 93/2, I-40129 Bologna, Italy*
[2]*INAF - Astrophysics and Space Science Observatory of Bologna, via Gobetti 93/3, I-40129 Bologna, Italy*
[3] *Dipartimento di Fisica "Aldo Pontremoli", Università degli Studi di Milano, via G. Celoria 16, I-20133 Milano, Italy*
[4]*Dipartimento di Fisica "G. Occhialini", Università degli Studi di Milano-Bicocca, Piazza della Scienza 3, I-20126 Milano, Italy*
[5]*INFN, Sezione di Milano-Bicocca, Piazza della Scienza 3, I-20126 Milano, Italy*
[6]*INAF - Osservatorio Astronomico di Brera, via Brera 20, 20121 Milano, Italy*

Alberto Sesana

Accepted XXX. Received YYY; in original form ZZZ

ABSTRACT

Extreme mass ratio inspirals (EMRIs) are compact binary systems characterized by a mass-ratio $q = m/M$ in the range 10^{-9}–10^{-4} and represent primary gravitational wave (GW) sources for the forthcoming Laser Interferometer Space Antenna (LISA). While their standard formation channel involves relaxation processes deflecting compact objects on very low angular momentum orbits around the central massive black hole, a number of alternative formation channels has been proposed, including binary tidal break-up, migration in accretion disks and secular and chaotic dynamics around a massive black hole binary (MBHB). In this work, we take an extensive closer look at this latter scenario, investigating how EMRIs can be triggered by a MBHBs, formed in the aftermath of galaxy mergers. By employing a suite of relativistic three-body simulations, we evaluate the efficiency of EMRI formation for different parameters of the MBHB, assessing the importance of both secular and chaotic dynamics. By modelling the distribution of compact objects in galaxy nuclei, we estimate the resulting EMRI formation rate, finding that EMRI are produced in a sharp burst, with peak rates that are 10-100 times higher than the standard two-body relaxation channel, lasting for 10^6–10^8 years. By coupling our results with an estimate of the cosmic MBHB merger rate, we finally forecast that LISA could observe $\mathcal{O}(10)$ EMRIs per year formed by this channel.

Key words: black hole physics – gravitational waves – celestial mechanics – methods: numerical

Riccardo Colombo

Matteo Bonetti

arXiv:2204.05343

What are EMRIs?

EMRIs features:

Binary systems with mass ratio between 10^{-9} and 10^{-4}

Formed by compact objects (COs)

A classical EMRI example is a binary system formed by **massive BH** + **stellar mass BH**

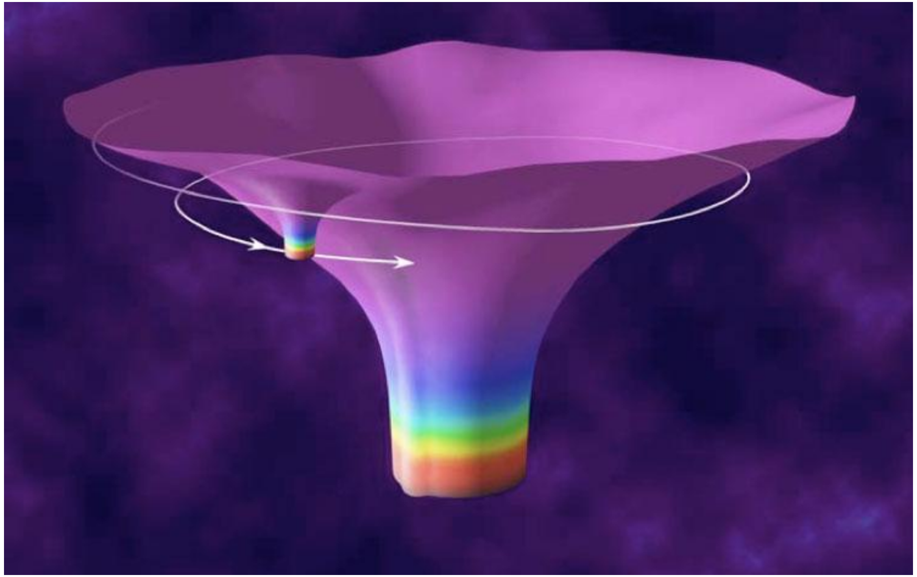

What are EMRIs?

Sesana & Colpi (2017)

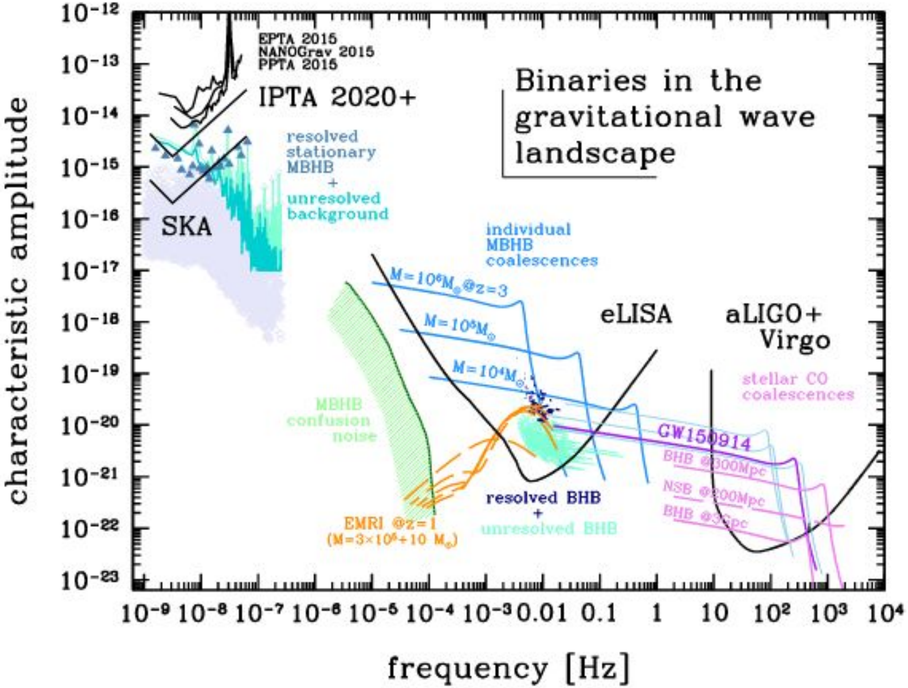

EMRIs will be primary GW sources for LISA science case

$$f_{GW,max} = 4 \times 10^{-3} \left(\frac{M}{10^6 M_\odot} \right)^{-1} Hz$$

$$h = \sqrt{\frac{32}{5}} \frac{(G\, M_c)^{5/3}}{c^4 d_L} (\pi f_{GW})^{2/3}$$

Why EMRIs are important?

The extreme mass-ratio makes the GW emission very inefficient

Orbital parameters of the binary

Redshifted MBH mass

Redshifted BH mass

Kerr quadrupole mass moment

Luminosity distance of the source

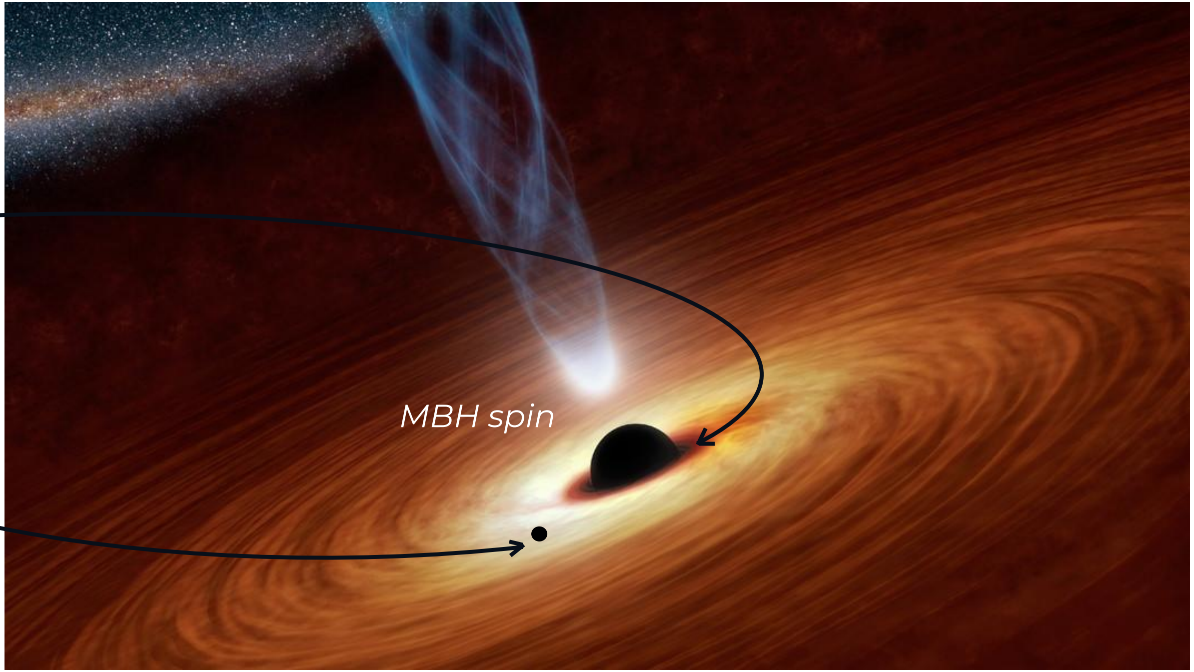

$10^4 - 10^5$ cycles → **Extremely precise measurements**

Why EMRIs are important?

Quadrupole mass moment	Luminosity distance	Inclination of the orbit	Significant number of EMRIs
↓	↓	↓	↓
Test for GR	Test for Cosmology	Test for the distribution of COs around the MBH	Constrain the MBH mass function

How do they form?

High densities → Dynamical interactions → Tidal Disruptions / Direct Plunge / EMRIs

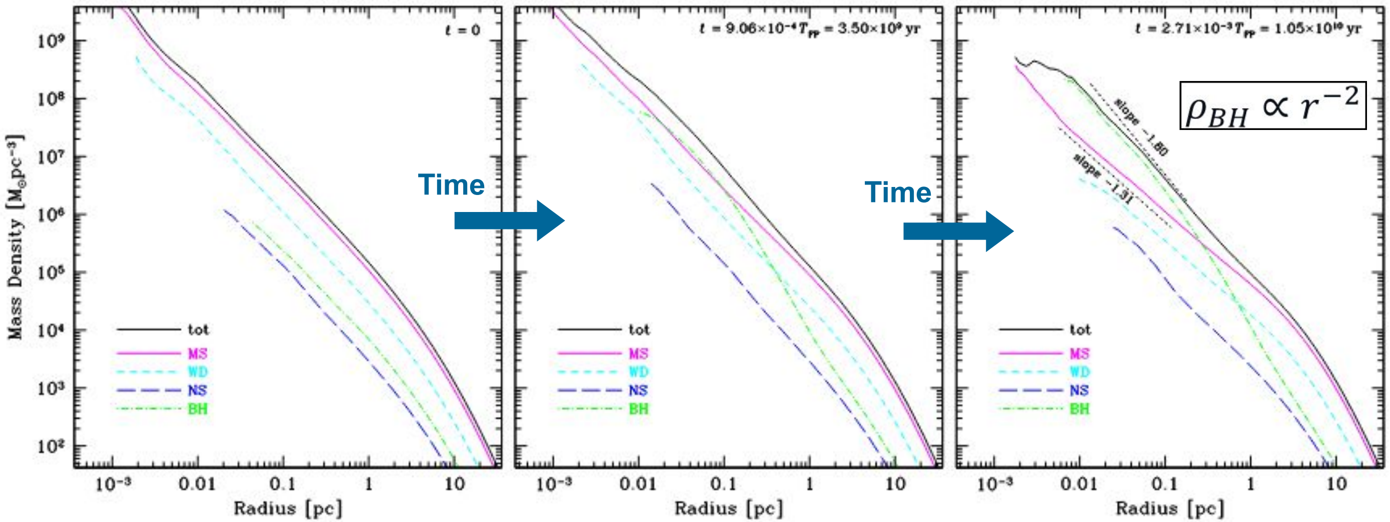

Freitag et al (2006)

How do they form?

Possible dynamical mechanism...

- Standard Channel: EMRI formation is consequence of two bodies relaxation

- Binary Tidal Breakup

- BH migration in the disk of AGNs

Amaro Seoane et al. (2018)

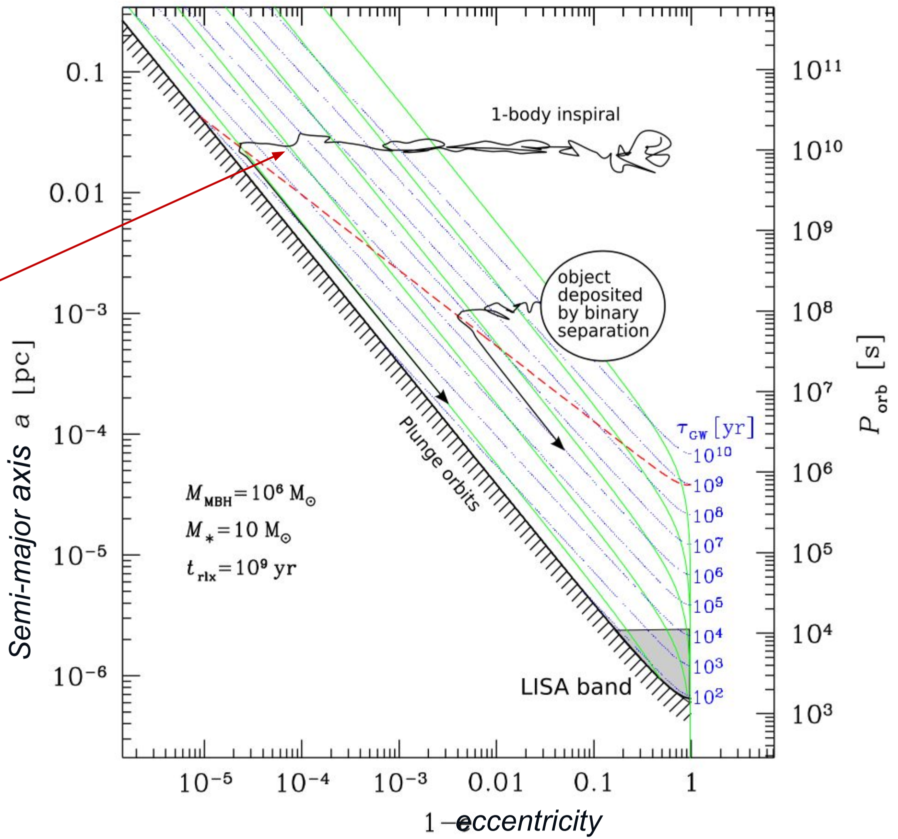

How do they form?

Possible dynamical mechanism...

- Standard Channel: EMRI formation is consequence of two bodies relaxation

- Binary Tidal Breakup

- BH migration in the disk of AGNs

Amaro Seoane et al. (2018)

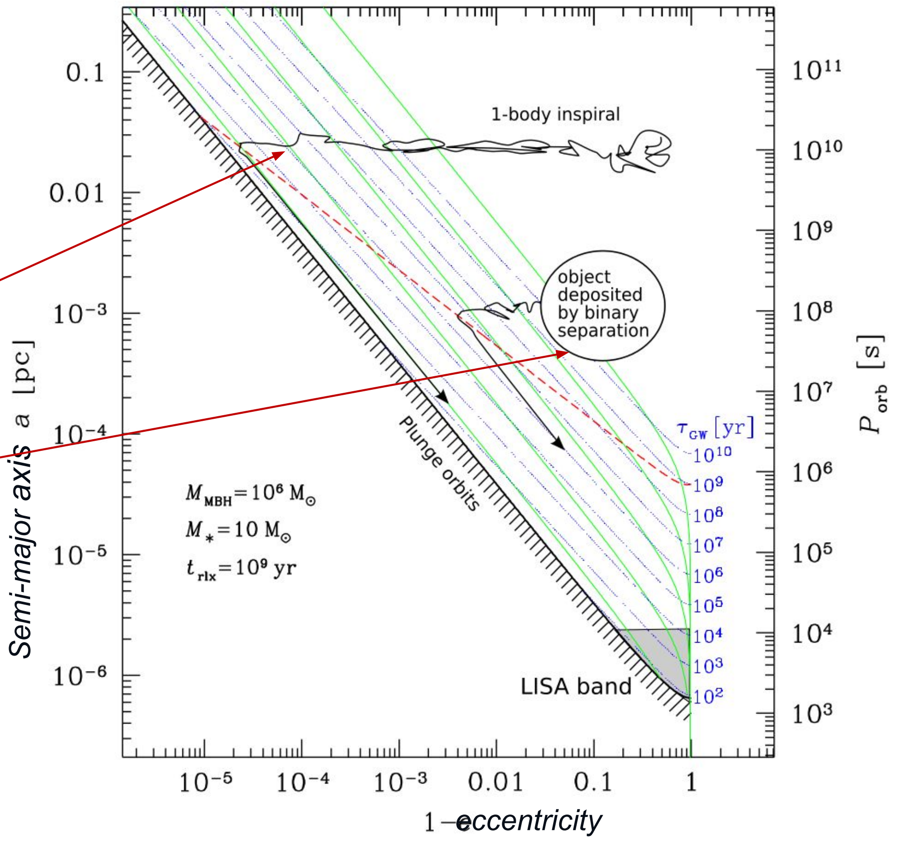

How do they form?

… another possibility

EMRI formation in a Massive Black Hole Binary (MBHB)

Investigated by Bode & Wegg +14 (with a number of simplifying assumptions) and recently by Naoz+22 (different setup, see next)

Dynamical Formation → Cosmological Rate → Detection Rate with LISA

MBHB Channel-Ingredients

We would like to simulate a system featuring:

- Primary MBH
- A cusp of stellar-mass CO around it
- A secondary MBH

We choose the semi-analytical way, i.e. we pick one CO at a time and simulate a series of three-body systems

(EMRI identified when GW timescale **smaller** than relaxation timescale)

MBHB Channel-Ingredients

Simulations set-up:

- Inner and outer binary : hierarchical triplet

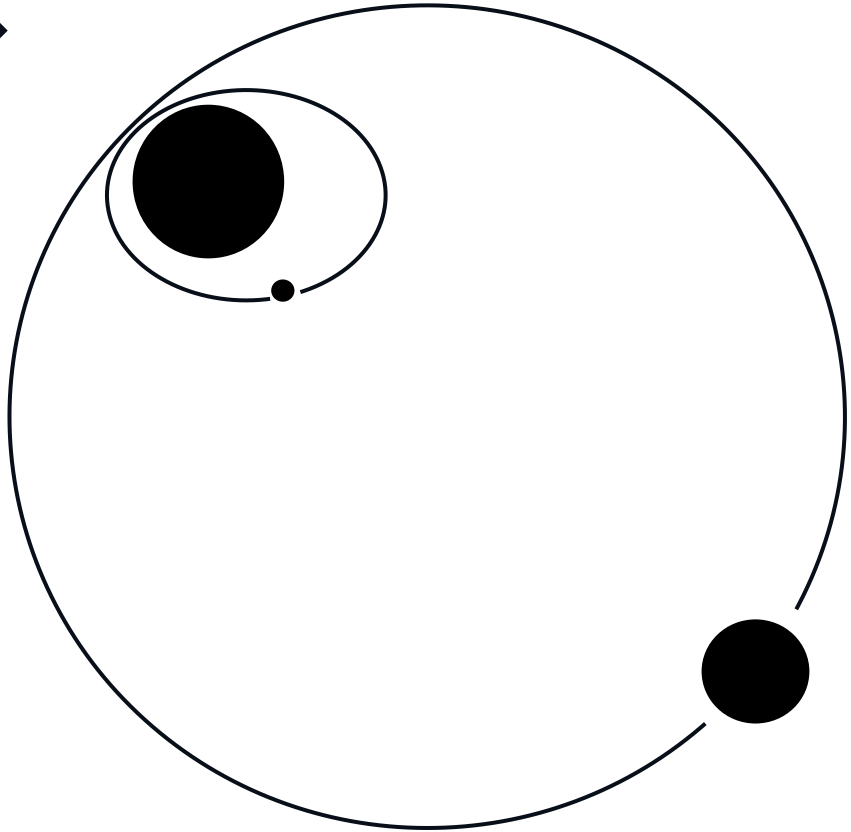

MBHB Channel-Ingredients

Simulations set-up:

- Inner and outer b hierarchical triple
- Post-Newtonian Evolution

Newtonian

$$H_0 = \frac{1}{2}\sum_{\alpha}\frac{|\vec{p}_\alpha|^2}{m_\alpha} - \frac{G}{2}\sum_{\alpha}\sum_{\beta\neq\alpha}\frac{m_\alpha m_\beta}{r_{\alpha\beta}}$$

1PN

$$\begin{aligned} H_1 = &-\frac{1}{8}\sum_{\alpha} m_\alpha\left(\frac{|\vec{p}_\alpha|^2}{m_\alpha^2}\right)^2 \\ &-\frac{G}{4}\sum_{\alpha}\sum_{\beta\neq\alpha}\frac{1}{r_{\alpha\beta}}\left[6\frac{m_\beta}{m_\alpha}|\vec{p}_\alpha|^2 - 7\vec{p}_\alpha\cdot\vec{p}_\beta - (\vec{n}_{\alpha\beta}\cdot\vec{p}_\alpha)(\vec{n}_{\alpha\beta}\cdot\vec{p}_\beta)\right] \\ &+\frac{G^2}{2}\sum_{\alpha}\sum_{\beta\neq\alpha}\sum_{\gamma\neq\alpha}\frac{m_\alpha m_\beta m_\gamma}{r_{\alpha\beta}r_{\alpha\gamma}} \end{aligned}$$

2.5PN

$$H_{2.5} = \frac{G}{45}\dot{\chi}_{(4)ij}(\vec{x}_{\alpha'},\vec{p}_{\alpha'};t)\chi_{(4)ij}(\vec{x}_\alpha,\vec{p}_\alpha)$$

$$\begin{aligned} H_2 = &\frac{1}{16}\sum_{\alpha} m_\alpha\left(\frac{|\vec{p}_\alpha|^2}{m_\alpha^2}\right)^3 + \frac{G}{16}\sum_{\alpha}\sum_{\beta\neq\alpha}\frac{(m_\alpha m_\beta)^{-1}}{r_{\alpha\beta}}\Bigg[10\left(\frac{m_\beta}{m_\alpha}|\vec{p}_\alpha|^2\right)^2 - 11|\vec{p}_\alpha|^2|\vec{p}_\beta|^2 - 2(\vec{p}_\alpha\cdot\vec{p}_\beta)^2 \\ &+ 10|\vec{p}_\alpha|^2(\vec{n}_{\alpha\beta}\cdot\vec{p}_\beta)^2 - 12(\vec{p}_\alpha\cdot\vec{p}_\beta)(\vec{n}_{\alpha\beta}\cdot\vec{p}_\alpha)(\vec{n}_{\alpha\beta}\cdot\vec{p}_\beta) - 3(\vec{n}_{\alpha\beta}\cdot\vec{p}_\alpha)^2(\vec{n}_{\alpha\beta}\cdot\vec{p}_\beta)^2\Bigg] \\ &+ \frac{G^2}{8}\sum_{\alpha}\sum_{\beta\neq\alpha}\sum_{\gamma\neq\alpha}\frac{1}{r_{\alpha\beta}r_{\alpha\gamma}}\Bigg[18\frac{m_\beta m_\gamma}{m_\alpha}|\vec{p}_\alpha|^2 + 14\frac{m_\alpha m_\gamma}{m_\beta}|\vec{p}_\beta|^2 - 2\frac{m_\alpha m_\gamma}{m_\beta}(\vec{n}_{\alpha\beta}\cdot\vec{p}_\beta)^2 \\ &- 50m_\gamma(\vec{p}_\alpha\cdot\vec{p}_\beta) + 17m_\alpha(\vec{p}_\beta\cdot\vec{p}_\gamma) - 14m_\gamma(\vec{n}_{\alpha\beta}\cdot\vec{p}_\alpha)(\vec{n}_{\alpha\beta}\cdot\vec{p}_\beta) \\ &+ 14m_\alpha(\vec{n}_{\alpha\beta}\cdot\vec{p}_\beta)(\vec{n}_{\alpha\beta}\cdot\vec{p}_\gamma) + m_\alpha(\vec{n}_{\alpha\beta}\cdot\vec{n}_{\alpha\gamma})(\vec{n}_{\alpha\beta}\cdot\vec{p}_\beta)(\vec{n}_{\alpha\gamma}\cdot\vec{p}_\gamma)\Bigg] \\ &+ \frac{G^2}{8}\sum_{\alpha}\sum_{\beta\neq\alpha}\sum_{\gamma\neq\alpha}\frac{1}{r_{\alpha\beta}^2}\Bigg[2m_\beta(\vec{n}_{\alpha\beta}\cdot\vec{p}_\alpha)(\vec{n}_{\alpha\gamma}\cdot\vec{p}_\gamma) + 2m_\beta(\vec{n}_{\alpha\beta}\cdot\vec{p}_\beta)(\vec{n}_{\alpha\gamma}\cdot\vec{p}_\gamma) \\ &+ \frac{m_\alpha m_\beta}{m_\gamma}\big(5(\vec{n}_{\alpha\beta}\cdot\vec{n}_{\alpha\gamma})|\vec{p}_\gamma|^2 - (\vec{n}_{\alpha\beta}\cdot\vec{n}_{\alpha\gamma})(\vec{n}_{\alpha\gamma}\cdot\vec{p}_\gamma)^2 - 14(\vec{n}_{\alpha\beta}\cdot\vec{p}_\gamma)(\vec{n}_{\alpha\gamma}\cdot\vec{p}_\gamma)\big)\Bigg] \\ &+ \frac{G^2}{4}\sum_{\alpha}\sum_{\beta\neq\alpha}\frac{m_\alpha}{r_{\alpha\beta}^2}\left[\frac{m_\beta}{m_\alpha}|\vec{p}_\alpha|^2 + \frac{m_\alpha}{m_\beta}|\vec{p}_\beta|^2 - 2(\vec{p}_\alpha\cdot\vec{p}_\beta)\right] \\ &+ \frac{G^2}{2}\sum_{\alpha}\sum_{\beta\neq\alpha}\sum_{\gamma\neq\alpha,\beta}\frac{(n^i_{\alpha\beta}+n^i_{\alpha\gamma})(n^j_{\alpha\beta}+n^j_{\gamma\beta})}{(r_{\alpha\beta}+r_{\beta\gamma}+r_{\gamma\alpha})^2}\Bigg[8m_\beta(p_{\alpha i}p_{\gamma j}) - 16m_\beta(p_{\alpha j}p_{\gamma i}) \\ &+ 3m_\gamma(p_{\alpha i}p_{\beta j}) + 4\frac{m_\alpha m_\beta}{m_\gamma}(p_{\gamma i}p_{\gamma j}) + \frac{m_\beta m_\gamma}{m_\alpha}(p_{\alpha i}p_{\alpha j})\Bigg] \\ &+ \frac{G^2}{2}\sum_{\alpha}\sum_{\beta\neq\alpha}\sum_{\gamma\neq\alpha,\beta}\frac{m_\alpha m_\beta m_\gamma}{(r_{\alpha\beta}+r_{\beta\gamma}+r_{\gamma\alpha})r_{\alpha\beta}}\Bigg[8\frac{\vec{p}_\alpha\cdot\vec{p}_\gamma - (\vec{n}_{\alpha\beta}\cdot\vec{p}_\alpha)(\vec{n}_{\alpha\beta}\cdot\vec{p}_\gamma)}{m_\alpha m_\gamma} \\ &- 3\frac{\vec{p}_\alpha\cdot\vec{p}_\beta - (\vec{n}_{\alpha\beta}\cdot\vec{p}_\alpha)(\vec{n}_{\alpha\beta}\cdot\vec{p}_\beta)}{m_\alpha m_\beta} - 4\frac{|\vec{p}_\gamma|^2 - (\vec{n}_{\alpha\beta}\cdot\vec{p}_\gamma)^2}{m_\gamma^2} - \frac{|\vec{p}_\alpha|^2 - (\vec{n}_{\alpha\beta}\cdot\vec{p}_\alpha)^2}{m_\alpha^2}\Bigg] \\ &- \frac{G^3}{2}\sum_{\alpha}\sum_{\beta\neq\alpha}\left(\sum_{\gamma\neq\alpha,\beta}\frac{m_\alpha^2 m_\beta m_\gamma}{r_{\alpha\beta}^2 r_{\beta\gamma}} + \frac{1}{2}\sum_{\gamma\neq\beta}\frac{m_\alpha^2 m_\beta m_\gamma}{r_{\alpha\beta}^2 r_{\beta\gamma}}\right) \\ &- \frac{3G^3}{8}\sum_{\alpha}\sum_{\beta\neq\alpha}\left(\sum_{\gamma\neq\alpha}\frac{m_\alpha^2 m_\beta m_\gamma}{r_{\alpha\beta}^2 r_{\alpha\gamma}} + \sum_{\gamma\neq\alpha,\beta}\frac{m_\alpha^2 m_\beta m_\gamma}{r_{\alpha\beta}^2 r_{\beta\gamma}}\right) \\ &- \frac{3G^3}{8}\sum_{\alpha}\sum_{\beta\neq\alpha}\sum_{\gamma\neq\alpha,\beta}\frac{m_\alpha^2 m_\beta m_\gamma}{r_{\alpha\beta}r_{\alpha\gamma}r_{\beta\gamma}} \\ &- \frac{G^3}{64}\sum_{\alpha}\sum_{\beta\neq\alpha}\sum_{\gamma\neq\alpha,\beta}\frac{m_\alpha^2 m_\beta m_\gamma}{r_{\alpha\beta}r_{\alpha\gamma}^3 r_{\beta\gamma}}\Bigg[18r_{\alpha\gamma}^2 - 60r_{\beta\gamma}^2 - 24r_{\alpha\gamma}(r_{\alpha\beta}+r_{\beta\gamma}) \\ &+ 60\frac{r_{\alpha\gamma}r_{\beta\gamma}^2}{r_{\alpha\beta}} + 56r_{\alpha\beta}r_{\beta\gamma} - 72\frac{r_{\beta\gamma}^3}{r_{\alpha\beta}} + 35\frac{r_{\beta\gamma}^4}{r_{\alpha\beta}^2} + 6r_{\alpha\beta}^2\Bigg] - \frac{G^3}{4}\sum_{\alpha}\sum_{\beta\neq\alpha}\frac{m_\alpha^2 m_\beta^2}{r_{\alpha\beta}^3}. \end{aligned}$$

2PN

We integrate the time evolution following the inner binary orbital timescale

MBHB Channel-Ingredients

Simulations set-up:

- Inner and outer binary : hierarchical triplet
- Post-Newtonian Evolution
- Stellar potential
- Hardening

$$\dot{a} = -a^2 \frac{GH\rho}{\sigma}$$
$$\dot{e} = a \frac{GHK\rho}{\sigma}$$

Added through a fictitious force in the direct 3-body integrator

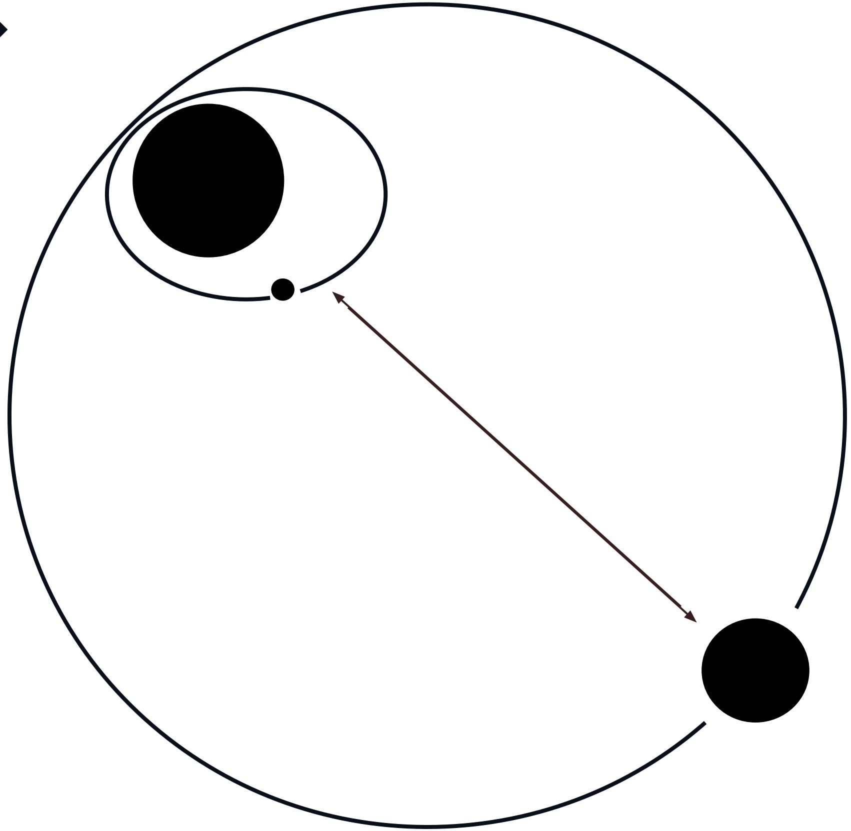

Stellar hardening

$$\dot{a} = -a^2 \frac{GH\rho}{\sigma}$$

$$\dot{e} = a\frac{GHK\rho}{\sigma}$$

Stellar hardening brings the secondary MBH closer to the inner binary.

The triplet's doom is the dynamical instability, a regime where secular theory cannot be employed

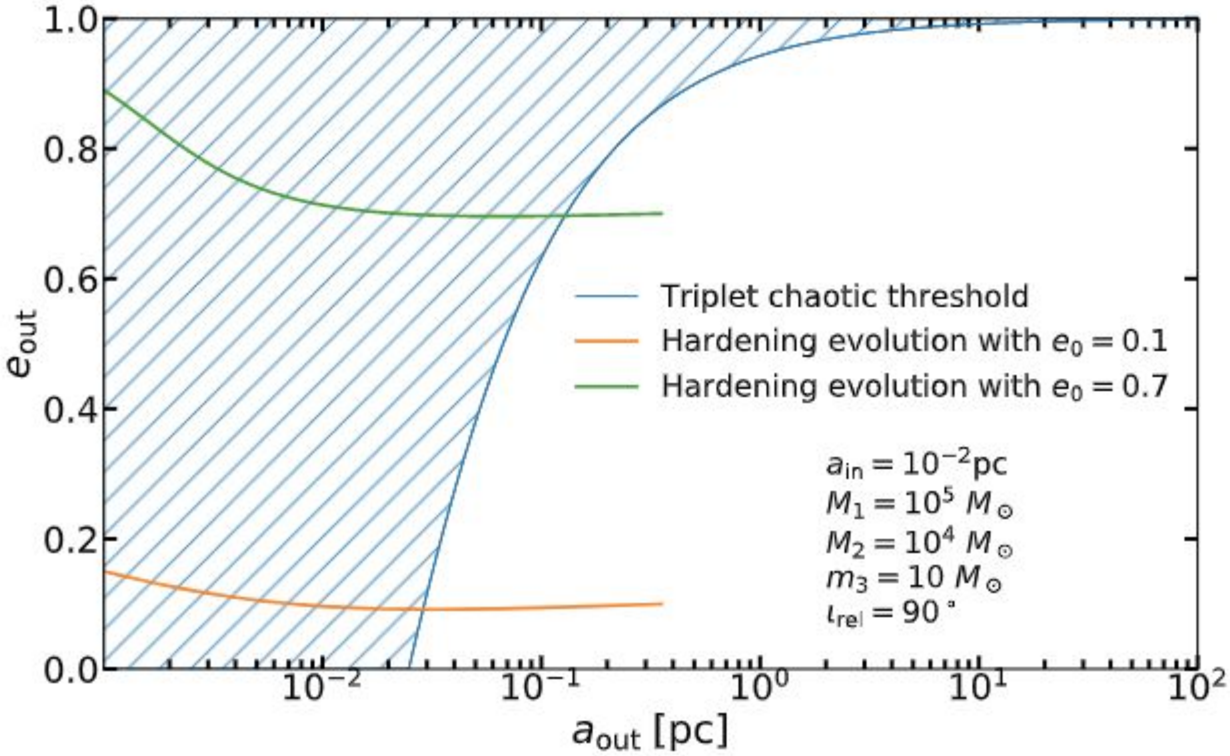

See Naoz+22 for a different approach considering the secular formalism

MBHB Channel

Interactions:

Secular

Lidov-Kozai oscillations

Exchange between relative inclination and eccentricity of the inner binary

<u>GR precession generally damp the process</u>

Relative separations between the three objects during one simulation

M1-M2 -> outer binary

M1-m3 -> inner binary

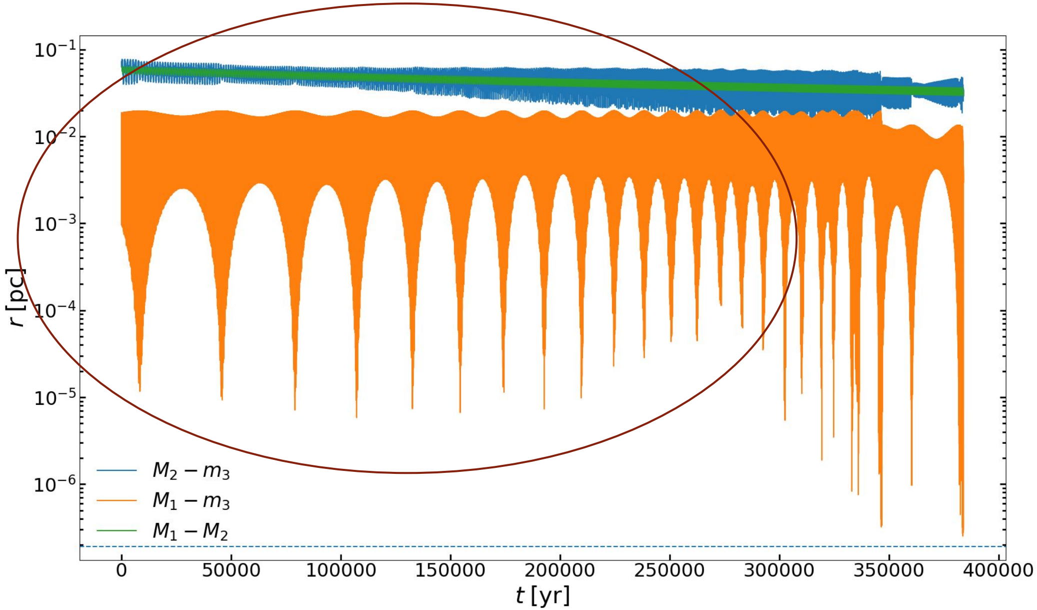

MBHB Channel

Interactions:

Chaotic

Hierarchy is lost

Strong encounters

Relative separations between the three objects during one simulation

M1-M2 -> outer binary

M1-m3 -> inner binary

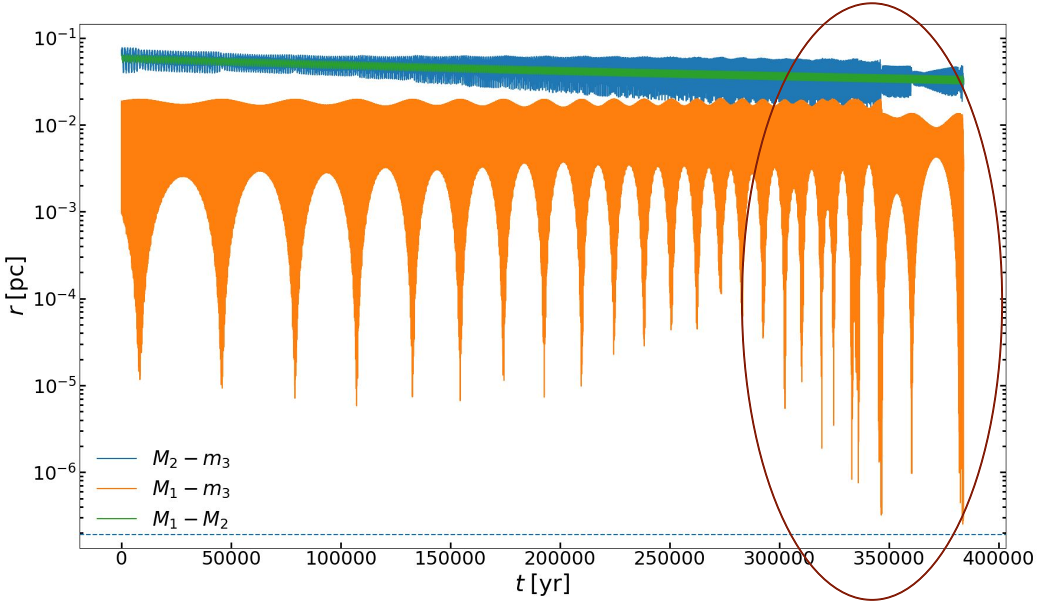

MBHB Channel

Parameter space:

Mass of the primary MBH M_1:

$3\text{x}10^5, 10^6, 3\text{x}10^6\ M_\odot$

MBHs mass ratio $q = M_2/M_1$:

0.003, 0.01, 0.03, 0.1

MBHB eccentricity e_{out}:

0.1 and 0.7

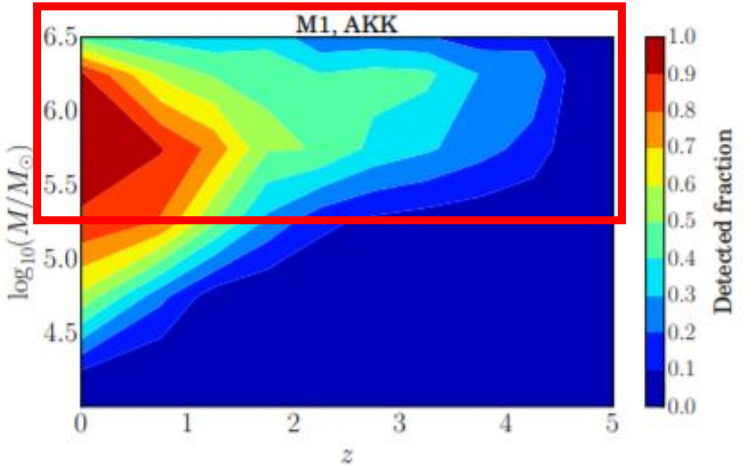

Expected EMRIs detected fraction with respect to the mass of the primary MBH and the redshift

Babak, Gair & Sesana (2017)

Grand total of 480.000 simulations

MBHB Channel

EMRI features:

Initial conditions

$M_1=3x10^5$ q=0.1 e_{out}=0.1

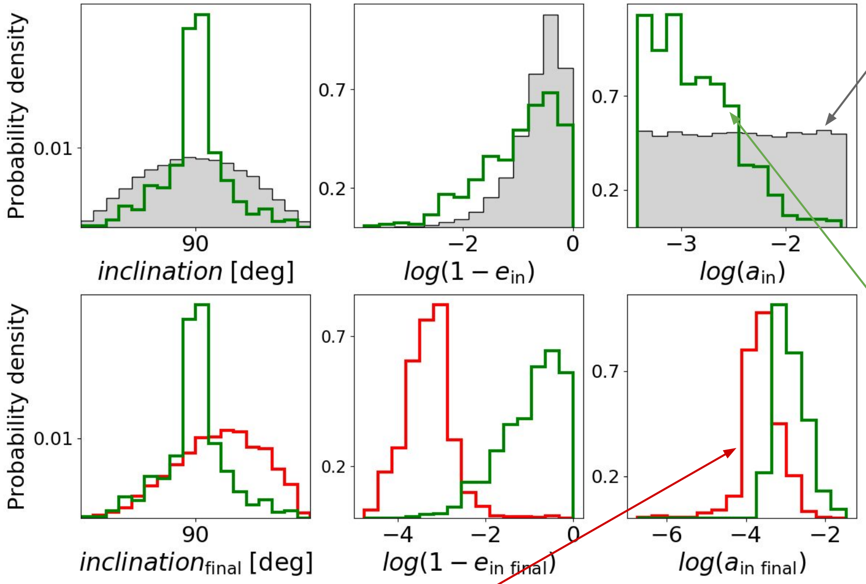

$M_1=3x10^5$ q=0.003 e_{out}=0.1

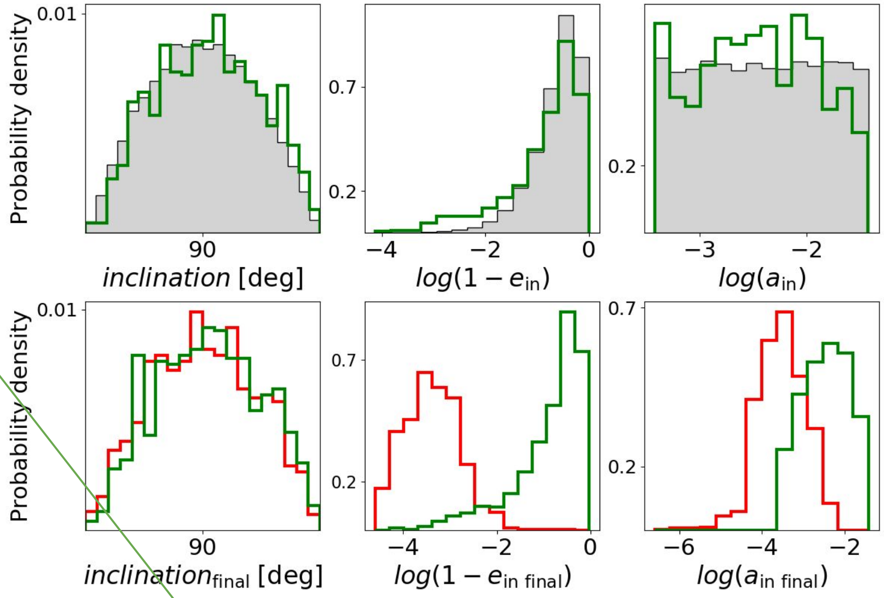

@ simulation end

Initial parameters of identified EMRIs

MBHB Channel

Number of EMRIs:

- Low q, high MBHB eccentricity

Chaotic Interactions

- High q, low MBHB eccentricity

Secular Interactions

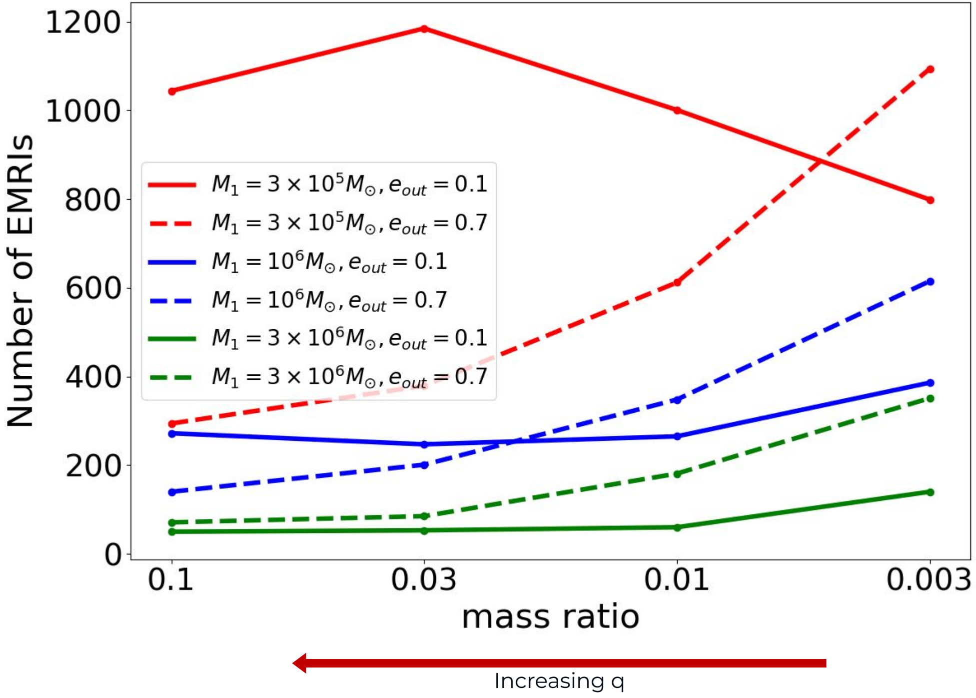

More EMRIs as q decreases

MBHB Channel

EMRIs formation rate for fixed MBHB

$$\boxed{\sim 10^{-6} - 10^{-5}\ yr^{-1}}$$

10-100 times larger

than the standard

two-body relaxation

channel!

$M_1 = 3\times10^5 M_\odot$ q	$e_{\mathrm{out},0}$	$N_{\mathrm{EMRI,SIS}}$	$\langle T_{\mathrm{tot}}\rangle$ [yr]	Rates [yr^{-1}]
0.1	0.1	43.7	5.5×10^6	2×10^{-5}
	0.7	11.4	3.7×10^6	5×10^{-6}
0.03	0.1	60.7	1.1×10^7	10^{-5}
	0.7	23.3	7.7×10^7	5×10^{-6}
0.01	0.1	82.3	1.6×10^7	8×10^{-6}
	0.7	45.0	1.7×10^7	4×10^{-6}
0.003	0.1	100.2	3.9×10^7	4×10^{-6}
	0.7	93.2	4.4×10^7	2×10^{-6}
$M_1 = 10^6 M_\odot$ q	$e_{\mathrm{out},0}$	$N_{\mathrm{EMRI,SIS}}$	$\langle T_{\mathrm{tot}}\rangle$ [yr]	Rates [yr^{-1}]
0.1	0.1	45.6	4.3×10^6	2×10^{-5}
	0.7	22.6	5.2×10^6	6×10^{-6}
0.03	0.1	58.9	8.8×10^6	10^{-5}
	0.7	41.5	1.0×10^7	6×10^{-6}
0.01	0.1	127.9	1.8×10^7	10^{-5}
	0.7	88.8	2.5×10^7	4×10^{-6}
0.003	0.1	222.5	5.7×10^7	5×10^{-6}
	0.7	218.2	6.6×10^7	4×10^{-6}
$M_1 = 3\times10^6 M_\odot$ q	$e_{\mathrm{out},0}$	$N_{\mathrm{EMRI,SIS}}$	$\langle T_{\mathrm{tot}}\rangle$ [yr]	Rates [yr^{-1}]
0.1	0.1	25.1	4.3×10^6	9×10^{-6}
	0.7	34.9	6.4×10^6	8×10^{-6}
0.03	0.1	59.9	8.9×10^6	10^{-5}
	0.7	54.0	1.2×10^7	7×10^{-6}
0.01	0.1	97.0	2.1×10^7	7×10^{-6}
	0.7	218.4	3.1×10^7	10^{-5}
0.003	0.1	274.9	7.2×10^7	6×10^{-6}
	0.7	362.1	9.8×10^7	5×10^{-6}

MBHB Channel

EMRIs formation rate for fixed MBHB

$$\boxed{\sim 10^{-6} - 10^{-5}\, yr^{-1}}$$

10-100 times larger

than the standard

two-body relaxation

channel!

In this channel we have an EMRIs **formation burst**!

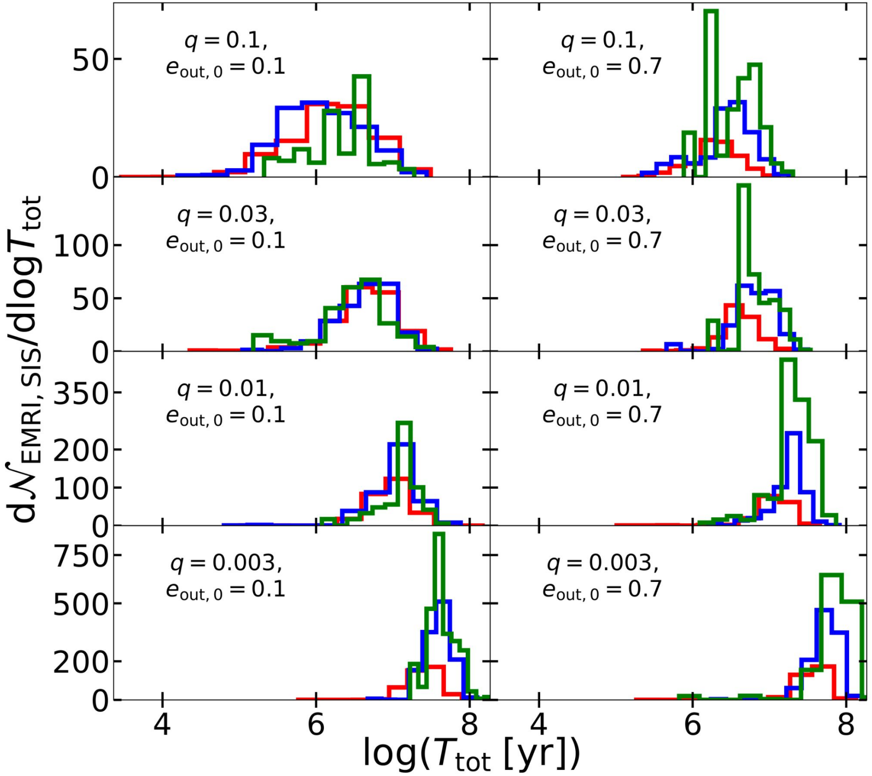

Time distribution of EMRIs formation. The three colors refer to the different values of M_1: M_1=3x10^5 M_1=10^6 M_1=3x10^6

Smaller q take longer

MBHB Channel

Cosmological EMRIs Formation Rate

MBHB Formation Rate

Semi Analytical

Cosmological model:

L-Galaxies

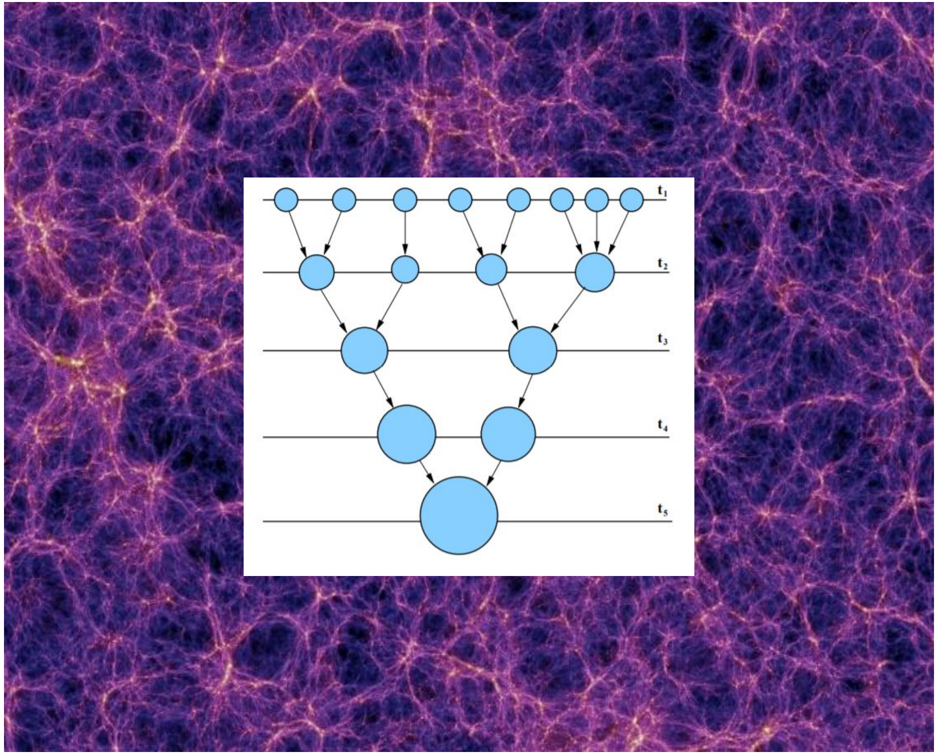

Note: No galactic delays in this version! MBHB merger rate could be slightly different

MBHB Channel

MBHB formation rate:

$\boxed{\sim 7\ yr^{-1}}$

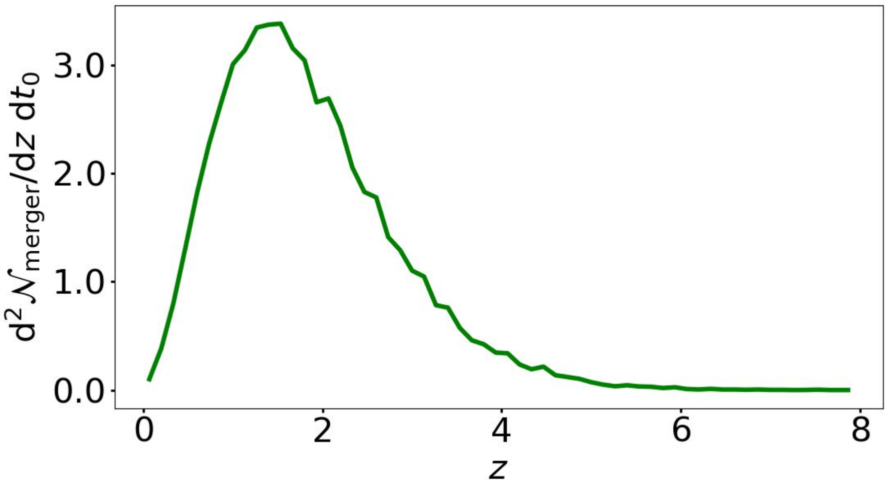

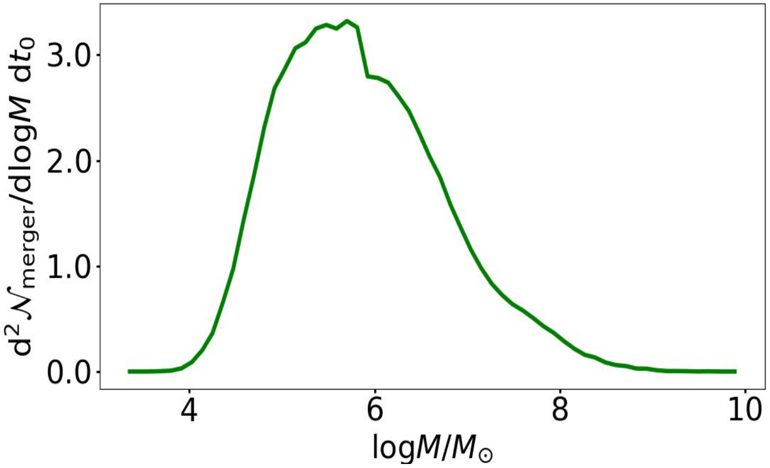

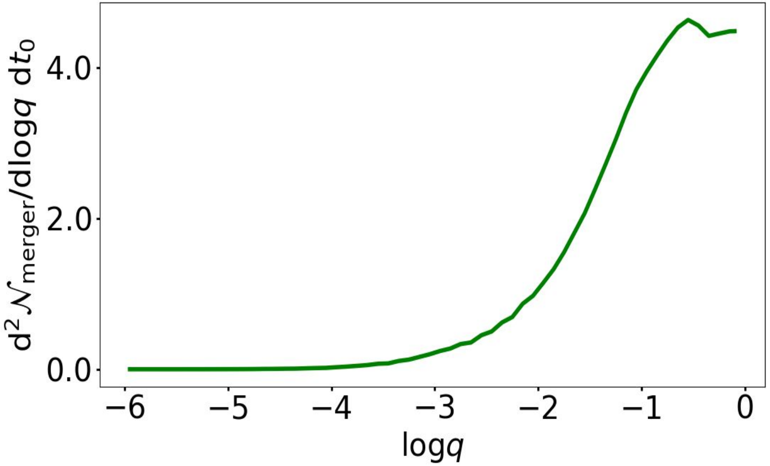

MBHB Channel

Cosmological EMRIs formation rate:

$\boxed{\sim 74\ yr^{-1}}$ for $e_{out} = 0.1$

$\boxed{\sim 64\ yr^{-1}}$ for $e_{out} = 0.7$

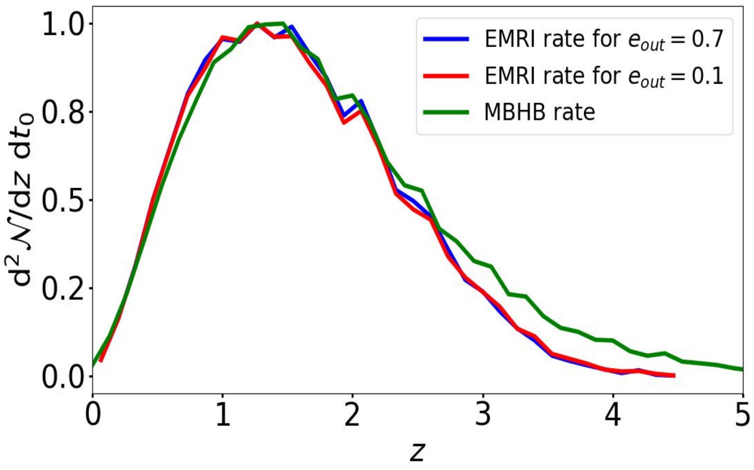

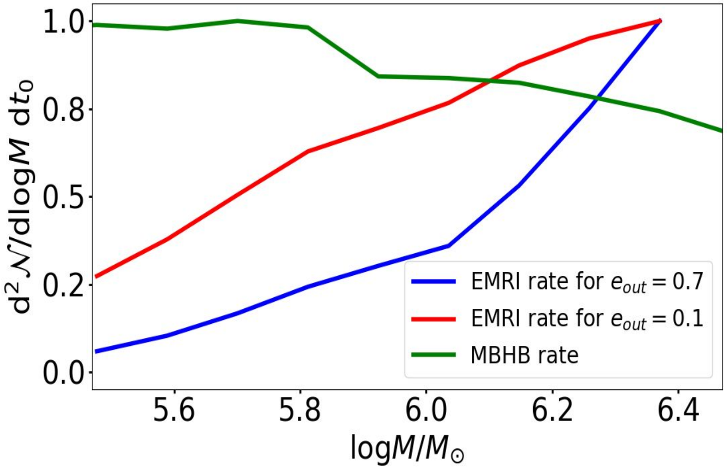

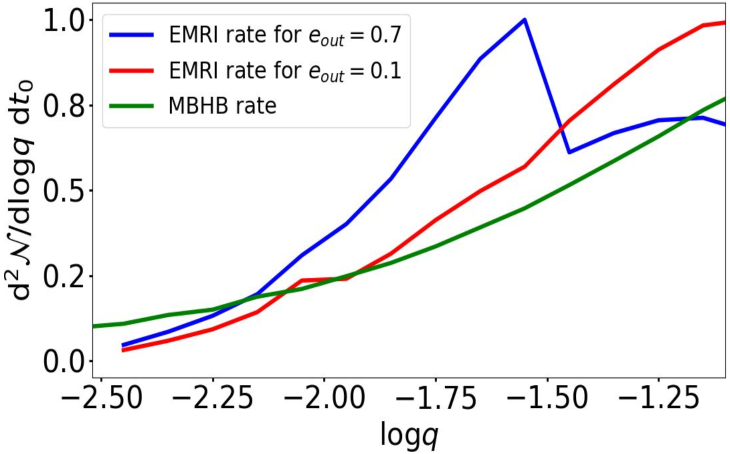

LISA

LISA requirement document (2018)

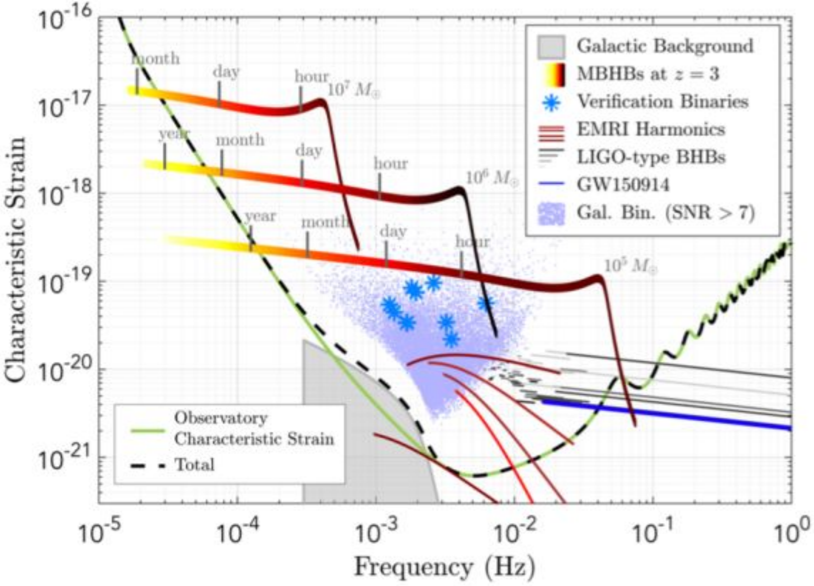

GW sources in the LISA band:

- **MBHB** $(10^4 < M_{MBH}/M_\odot < 10^7)$ coalescence out to $z > 20$
- **IMBHB** $(10^2 < M_{IMBH}/M_\odot < 10^4)$ coalescence out to $z > 10$
- **EMRIs** out to $z\sim2-3$
- Early steages of **COs binaries** evolution

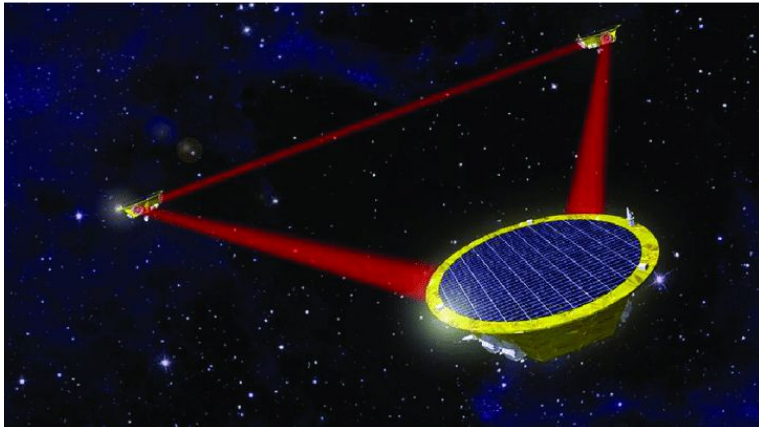

MBHB Channel

EMRI detection with LISA → SNR > 20

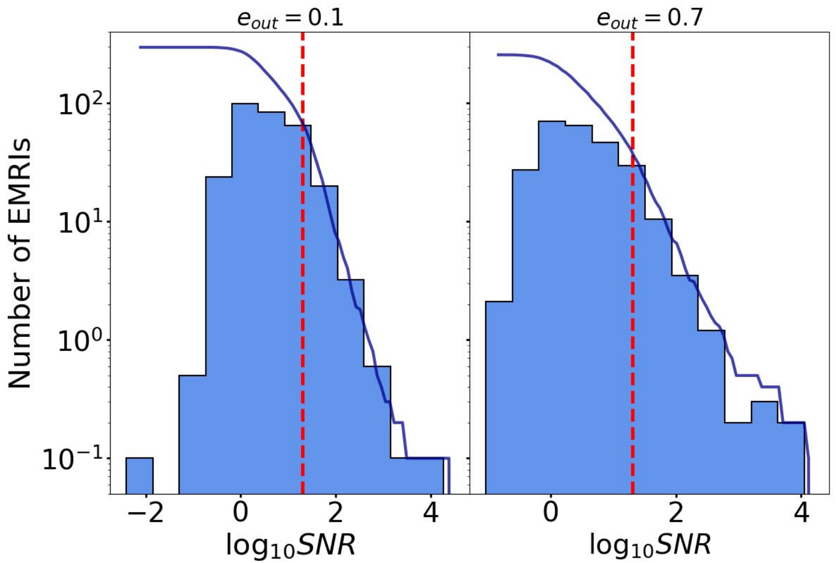

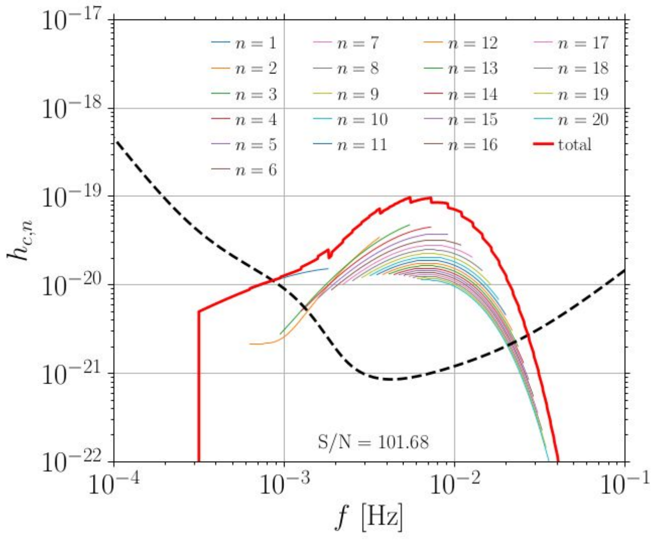

Bonetti & Sesana (2020)

Detected fraction:

42 on 296 EMRIs (15%) for $e_{out} = 0.1$

27 on 256 EMRIs (10%) for $e_{out} = 0.7$

During **4 yrs** of LISA mission

Conclusions and Future Perspectives

- The formation rate from the single MBHB is 10-100 greater with respect to the standard channel
- There is an EMRIs formation burst
- The MBHB channel is not negligible (10% of all detectable the EMRIs)

- Implementation of the code also with spinning MBHs and stochastic kicks
- Introduce different stellar potential
- Wider parameter space
- Use the results of a SAM implemented also with the MBHB dynamics
- Investigate any distinctive properties of EMRIs from this MBHB channel (high eccentricity? preferred inclination? perturbation in the GW waveform?.....)

EM Counterpart?

Quasi-Periodic Eruptions (QPE, Miniutti+19, Giustini+20, Arcodia+21,22)

- Tidal stripping of the He envelope of a massive star (Wang+19)
- WDs on high ecc orbit filling up their Roche lobes and feeding the MBHs during their pericenter passages (King20, Chen+22, King22)
- Main sequence star undergoing stable or unstable mass transfer (Krolik+22, Linian+22)
- Multiple EMRIs interacting among them (Metzger+22)

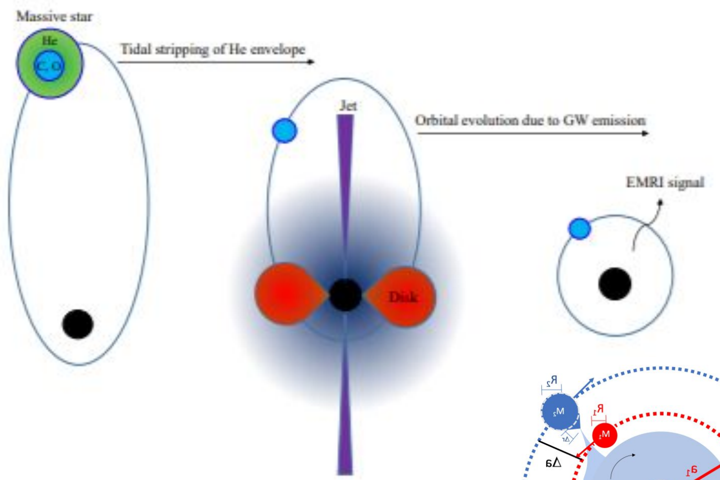

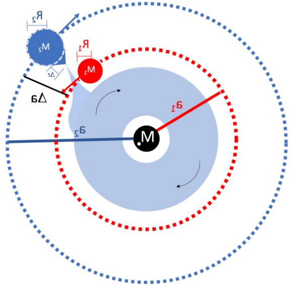

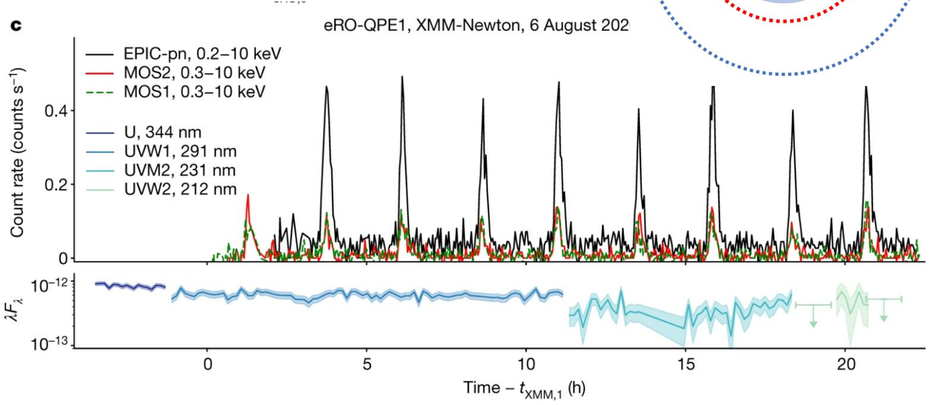

MBHB Channel

On average we can expect around ~10 detections per yr from this channel, with most of them concentrated at smaller primary masses

LISA sensitivity selects low primary masses

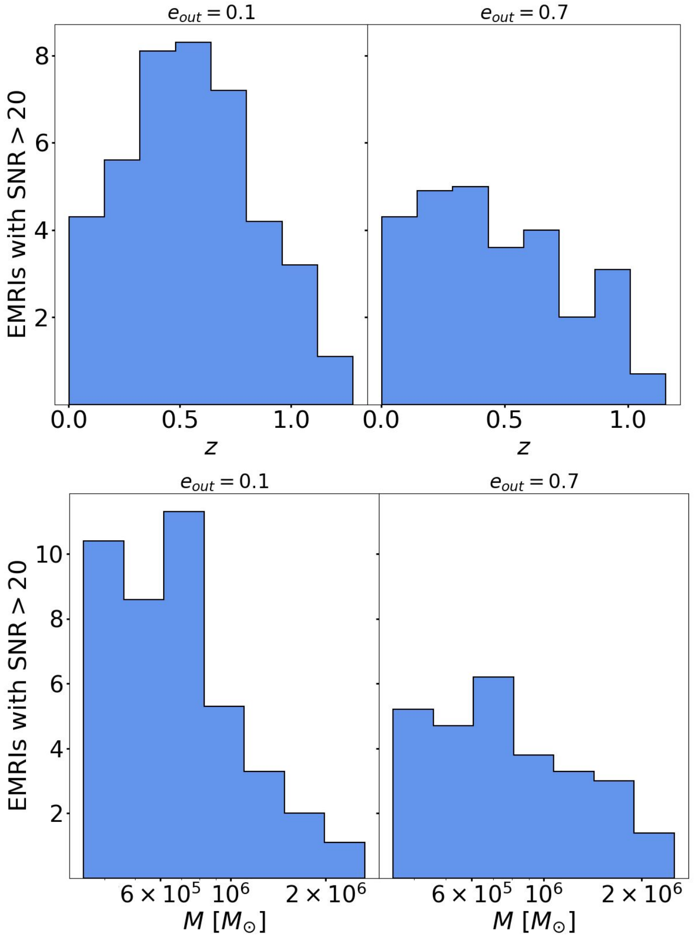

EMRI rates for SIS

SIS density profile:

$$\rho_{\rm BH} = \frac{\sigma^2}{2\pi G r^2}.$$

BH number per semi-major axis interval:

$$\frac{dN_{\rm BH,SIS}}{da} = \int_0^{2\pi}\int_0^{\pi} \frac{\rho_{\rm BH}(a)}{m_{\rm BH}} a^2 \sin\theta d\theta d\phi = \frac{2\sigma^2}{m_{\rm BH}G},$$

$$N_{\rm BH,SIS}(a) = \frac{2\sigma^2}{m_{\rm BH}G}a.$$

If we now divide the variability range of the BH's semi-major axis in 20 log bins equally spaced, with separations x_j, x_{j+1}, the number of BHs in the j-th bin will be:

$$N_{\rm BH,SIS}(j) = \frac{2\sigma^2}{m_{\rm BH}G}(10^{x_{j+1}} - 10^{x_j}).$$

Using the following proportion:

$$N_{\rm EMRI,SIS}(j) : N_{\rm BH,SIS}(j) = N_{\rm EMRI,sim}(j) : N_{\rm BH,sim}$$

and defining the weights:

$$w_j = \frac{N_{\rm BH,SIS}(j)}{N_{\rm BH,sim}},$$

we finally obtained the expected number of EMRIs in a SIS-like cusp starting from those detected in simulations:

$$N_{\rm EMRIs,SIS} = \sum_j N_{\rm EMRI,sim}(j)\, w_j.$$

Equation summary

Relaxation time

$$t_{\rm rlx} = 1.2 \times 10^{11} \left(\frac{\sigma}{100 \rm kms^{-1}} \right)^{7.47} \rm yr$$

Segregation Time

$$t_{\rm sgr} = (0.1 - 0.25)\ t_{\rm rlx}$$

Condition for EMRI identification

$$T_{\rm GW}(a, e) \leq (1 - e) t_{\rm rlx}$$

Evolution with GW emission

$$\begin{cases} \dfrac{de}{dt} = -\dfrac{304}{15} \dfrac{G^3 \mu M^2}{c^5 a^4 (1 - e^2)^{-5/2}} \left(e + \dfrac{121}{304} e^3 \right) \\ \dfrac{da}{dt} = -\dfrac{64}{5} \dfrac{G^3 \mu M^2}{c^5 a^3} F(e) \end{cases}$$

LK oscillations

$$\sqrt{1 - e_{\rm in}^2} \cos(\iota_{\rm rel})$$

GR precession

$$\delta\omega_{\rm GR} = \frac{6\pi G(M_1 + m_3)}{a_{\rm in}(1 - e_{\rm in})^2 c^2} + \frac{3\pi G^2 (18 + e_{\rm in}^2)(M_1 + m_3)^2}{2 a_{\rm in}^2 (1 - e_{\rm in}^2)^2 c^4}$$

Hardening equations

$$\begin{cases} \dot{a} = -a^2 \dfrac{G\rho H}{\sigma} \\ \dot{e} = a \dfrac{G\rho H K}{\sigma} \end{cases}$$

Stellar hardening

$$\dot{a} = -a^2 \frac{GH\rho}{\sigma}$$

$$\dot{e} = a \frac{GHK\rho}{\sigma}$$

We need to initialise the system into hierarchical configuration, but we also want to be efficient and we start integration at

$$a_{\rm out} = 2a_{\rm chaos}(a_{\rm in}, e_{\rm out})$$

the initial eccentricity is chosen at binary formation thus we assign the eccentricity according to the hardening tracks

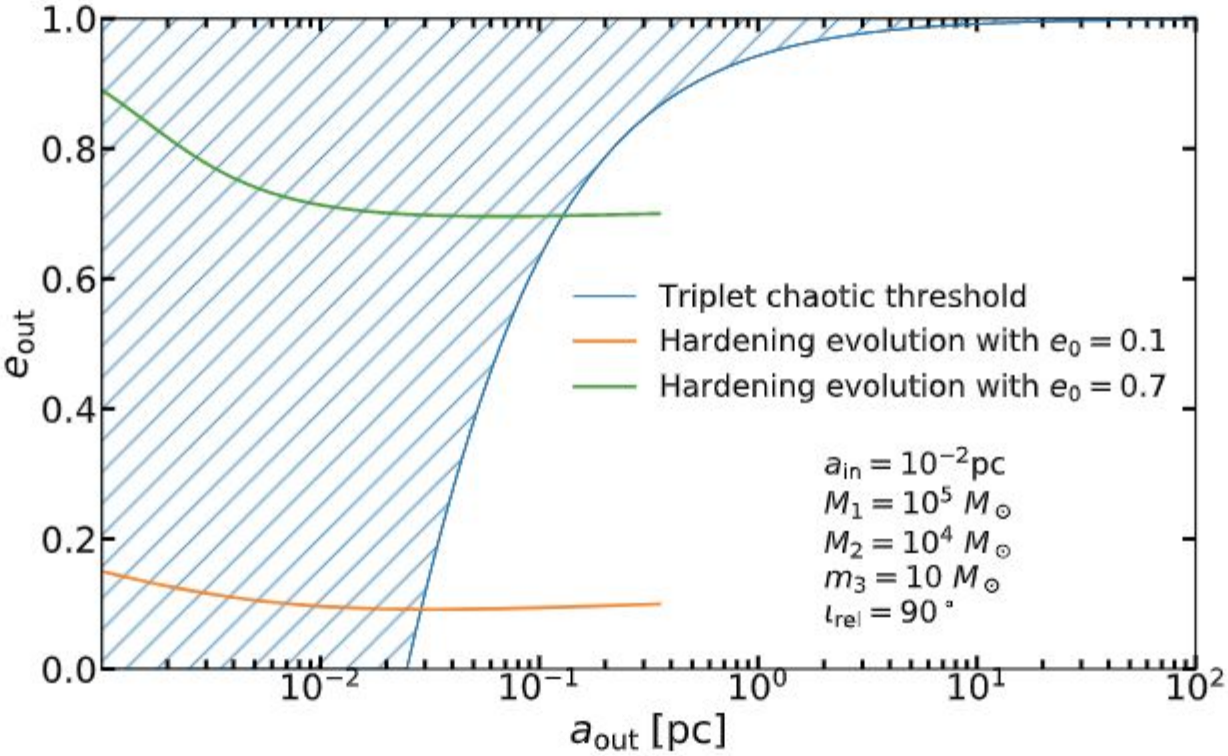

MBHB Channel

EMRI features:

M_1=3x10^5 q=0.1 e_{out}=0.1

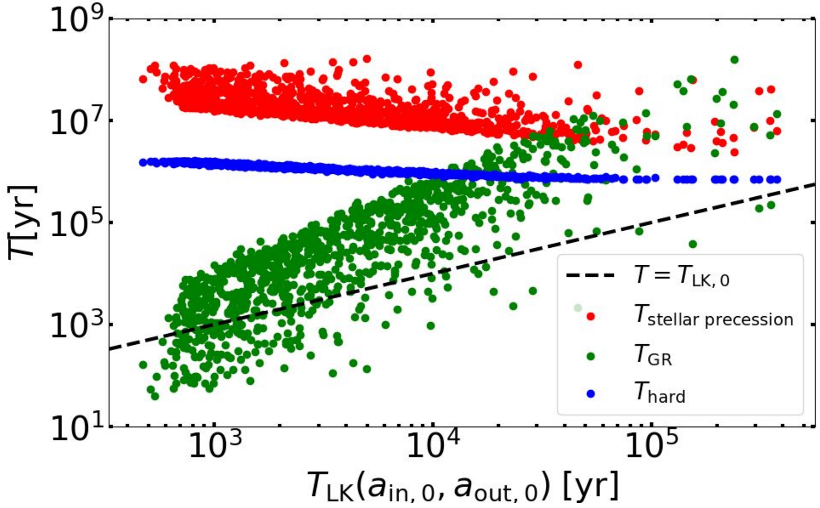

M_1=3x10^5 q=0.003 e_{out}=0.1

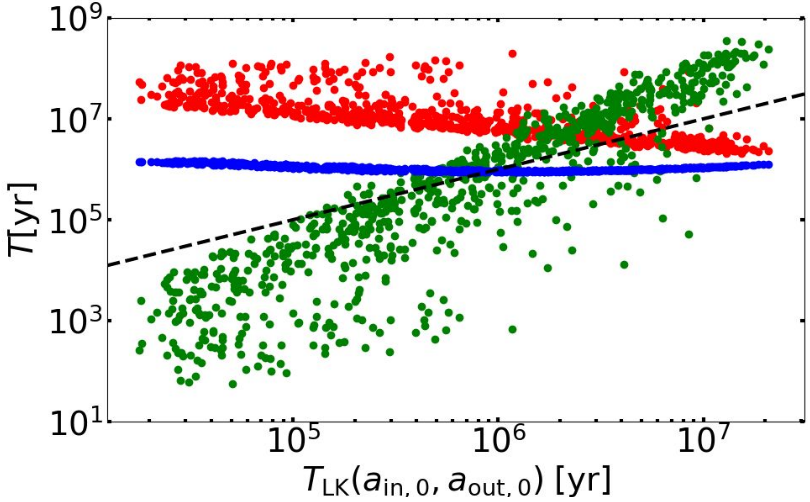

$$T_{\rm LK} = \frac{2}{3\pi}\frac{M_1}{M_2}\frac{P_{\rm out}^2}{P_{\rm in}}(1-e_{\rm out}^2)^{3/2} \propto \frac{1+q}{q}.$$

$$T_{\rm hard} = \frac{\sigma_{\rm inf}}{G\rho_{\rm eff,inf}}\int_{a_{\rm in,0}}^{a_{\rm out,0}}\frac{da}{a^2H(a)},$$

$$T_{\rm GR} = \frac{\pi}{\delta\omega_{\rm GR}}P_{\rm in},$$

$$T_{\rm star} = \frac{\pi}{\delta\omega_{\rm star}}P_{\rm in},$$

Simulation outcomes

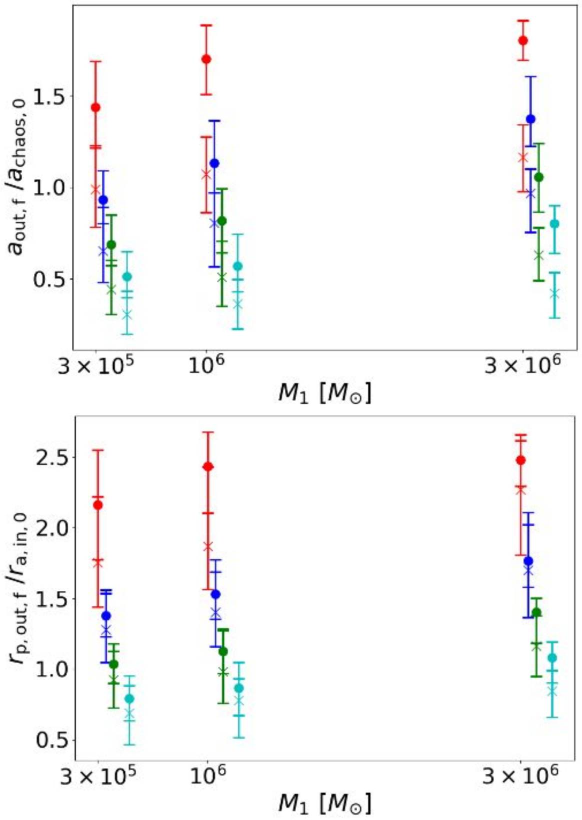

$M_1 = 3\times10^5 M_\odot$ q	$e_{\rm out,0}$	EMRIs	DPs	Swap	Ejections	Unresolved
0.1	0.1	1044	2466	7568	8921	1
	0.7	294	157	6937	12613	0
0.03	0.1	1185	2279	4923	11608	5
	0.7	379	211	5432	13978	0
0.01	0.1	1001	1180	4797	13012	10
	0.7	612	399	5237	13751	1
0.003	0.1	799	584	5958	12616	43
	0.7	1094	558	5590	12750	8

$M_1 = 10^6 M_\odot$ q	$e_{\rm out,0}$	EMRIs	DPs	Swap	Ejections	Unresolved
0.1	0.1	272	2391	8031	9324	0
	0.7	140	206	7016	12638	0
0.03	0.1	247	2194	5379	12180	0
	0.7	201	283	5441	14075	0
0.01	0.1	265	1231	5020	13480	4
	0.7	348	518	5338	13796	0
0.003	0.1	386	683	6315	12606	10
	0.7	615	737	6011	12631	6

$M_1 = 3\times10^6 M_\odot$ q	$e_{\rm out,0}$	EMRIs	DPs	Swap	Ejections	Unresolved
0.1	0.1	50	2115	8515	9320	0
	0.7	71	282	6837	12810	0
0.03	0.1	53	1851	5704	12391	1
	0.7	85	335	5563	14017	0
0.01	0.1	60	1059	5498	13383	0
	0.7	181	602	5391	13825	1
0.003	0.1	140	844	6770	12245	1
	0.7	351	922	6452	12275	0

Table 1. Final outcomes of the simulations divided according to the mass of the primary, the mass-ratio and the initial outer eccentricity. The last column contains the number of simulations that kept reaching the integration time limit of 150 minutes after three restarts, which are discarded.